

Metallization of Molybdenum Diselenide under Nonhydrostatic Compression

Bao Liu,* Lin Lin, Yang Gao, Yanzhang Ma, Pengyu Zhou, Dandan Han, and Chunxiao Gao*

Cite This: *J. Phys. Chem. C* 2021, 125, 5412–5416

Read Online

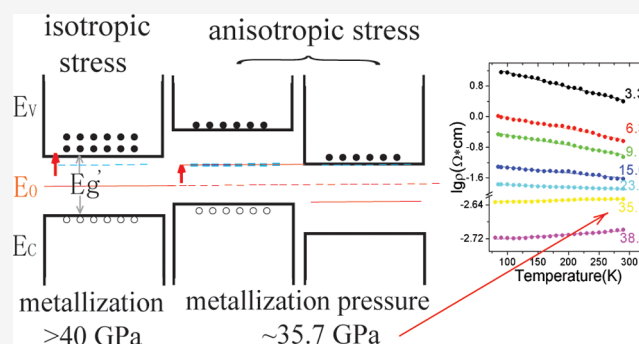
HPSTAR
1164-2021

ACCESS |

Metrics & More

Article Recommendations

ABSTRACT: It is known that metallization can greatly facilitate chemical reactions and dramatically change electric transport properties of materials. The search for materials displaying metallization at low pressure is one of the most urgent challenges. In this paper, pressure-induced metallization of molybdenum diselenide (MoSe_2) under nonhydrostatic compression has been studied experimentally using Hall effect and X-ray diffraction measurements combined with diamond anvil cell techniques. *In situ* conductivity and Hall effect measurements under pressure reveal a monotonic decrease of resistivity mostly related to a significant increase of the carrier density by a factor of 4. Above 35.7 GPa, the sample acquires a metallic character with a characteristic increase of the mobility from 9.9 to $16.2 \text{ cm}^2 \text{ V}^{-1} \text{ s}^{-1}$ and saturation of the carrier concentration at $5.1 \times 10^{20} \text{ cm}^{-3}$. These results show that the metallization of powder MoSe_2 can be initiated by a reduced pressure of 35.7 GPa under nonhydrostatic compression, compared to that above 40 GPa with a single-crystal sample under hydrostatic compression [*Nat. Commun.* 2015, 6, 7312]. The mechanisms of anisotropic-stress-induced metallization for such reduced initiation pressure have been discussed.



1. INTRODUCTION

Transition-metal dichalcogenides (TMD), MX_2 ($M = \text{Mo}, \text{W}, \text{Ti}, \text{Nb}, \text{Ta}, \text{etc.}, X = \text{S}, \text{Se}, \text{Te}, \text{etc.}$) have been subjected to many theoretical and experimental studies because of their continuously tunable electronic structures and band gaps. The structures of TMDs share a quasi-laminar model of two-dimensional (2D) sheets stacked on top of one another. Each sheet consists of three layers, a transition-metal atom layer in the middle and two chalcogen atom layers covalently bonded to the transition-metal atoms as the top and bottom layers.¹ These sheets are held together by weak van der Waals forces and show excellent mechanical properties such as high lubrication.² The combination of the covalent bonds within layers and van der Waals interactions between sheets results in highly anisotropic physical properties in TMDs. Such characteristic is of great significance in various applications, such as hydrogen evolution reaction catalysis,^{3,4} 2D monolayer solar cells,⁵ and ultrafast lithium-ion storage batteries.⁶ Furthermore, several methods, including intercalation, layer confinement, chemical vapor deposition, and stress, have been proved valid in the continuous modification of the electric properties of TMDs and affecting the performance of TMD devices.⁷ Thus, features have dramatically extended the potential applications of TMD materials in various areas.

As a promising candidate for solar cells,⁸ vast investigations in optical, structural, and electronic responses of MoSe_2 have

been performed using both experimental and theoretical methods.^{9–11} Sugai et al. measured the *in situ* high-pressure Raman spectra of MoSe_2 and showed that no clear indication of structural phase transition of MoSe_2 was discovered up to 16 GPa.¹² Aksoy et al. carried out *in situ* high-pressure X-ray diffraction (XRD) measurements of MoSe_2 and illustrated that no structural phase transformation occurred up to 35.7 GPa.¹³ Dave et al. examined the variation of electrical resistance of single-crystal MoSe_2 with pressure and discovered no abnormal behavior up to 6.5 GPa.¹⁴ However, previous theoretical calculations have predicted that the electronic properties of MoSe_2 can be altered in a controllable manner by applying hydrostatic pressure during the metallization process from 28 to 40 GPa while maintaining the 2H_c structure.¹⁵ Recently, such prediction has been verified experimentally by Zhao et al.,¹⁶ whose work shows that single crystals of MoSe_2 metalize without any structural transition at pressures above 40 GPa under hydrostatic compression. Such discovery suggests that

Received: January 12, 2021

Revised: February 9, 2021

Published: February 25, 2021



continuously tuning TMD materials' electronic structure by means of pressure is feasible and of great potential in optoelectronic and photovoltaic applications.

Meanwhile, diverse behaviors under different stress conditions are commonly observed in laminar or quasi-laminar materials, such as 2D graphene,¹⁷ WS₂,¹⁸ and MoS₂.^{19–21} The WS₂ powder undergoes isostructural 2H_c to 2H_a metallization under nonhydrostatic conditions, which is not observed under hydrostatic conditions.¹⁸ The total energy calculation predicted that monolayer 2H-MoS₂ remains stable till 67.9 GPa,¹⁹ whereas *in situ* pressure and temperature-dependent electrical resistivity measurements by Nayak et al. indicated that multilayer MoS₂ undergoes an electronic transition from a semiconductive to a metallic state at 19 GPa under hydrostatic compression.²⁰ Yet, as reflected in another *in situ* pressure-dependent resistivity measurements with no pressure-transmitting medium, MoS₂ powder samples first underwent an isostructural phase transition from a 2H_c to 2H_a structure, after which they became metallic at 28 GPa.²¹ These studies all suggest that the behaviors of TMD materials depend on both the state of stress and the morphology of the sample. Despite the intriguing diversity of TMD materials' response to different stress conditions, whether such regulation applies to MoSe₂ and the mechanisms behind it remain unclear.

In this paper, the abovementioned issues were addressed by combining *in situ* electrical transport measurements with *in situ* synchrotron XRD measurements in powder MoSe₂ under nonhydrostatic compression. The results indicate that the metallization of MoSe₂ can be initiated at a reduced pressure of 35.7 GPa under nonhydrostatic compression compared to that under hydrostatic compression (>40 GPa). The *in situ* Hall effect measurements, on the other hand, provided a deeper interpretation for the anisotropic-stress-induced metallization.

2. EXPERIMENTAL METHODS

The commercially available MoSe₂ powder (Alfa Co., purity of 99.8%) was loaded into a nonmagnetic diamond anvil cell with the anvil culet of 400 μm diameter. A sheet of rhenium used as a gasket was preindented to 40 μm thickness. A hole with 200 μm diameter was drilled at the center of the indentation by an electric discharge machine and served as the sample chamber. A piece of a ruby chip of around 5 μm was used for pressure calibration. A four-probe Mo film microcircuit with a van der Pauw configuration was used for *in situ* electrical transport measurements under pressure. The electrode manufacturing, electrical insulation, magnetic calibration, and other relevant experimental details have been reported in our previous studies.^{22–24} The sample thickness under pressure was measured by a micrometer with the accuracy of 0.5 μm , during which the deformation of the anvils was included as a correction.²⁵

In situ high-pressure XRD experiments were carried out using a synchrotron X-ray source ($\lambda = 0.6199 \text{ \AA}$) at the 4W2 High-Pressure Station of Beijing Synchrotron Radiation Facility (BSRF). The diffraction data were collected using an MAR165 CCD. The intensity versus diffraction angle patterns were generated from XRD images using FIT2D software. For nonhydrostatic compression and better electrode contact, no pressure-transmitting medium was used in both XRD measurements and Hall effect measurements. Although extensive efforts have been dedicated to generating the hydrostatic pressures in a diamond anvil cell by choosing various pressure mediums, this experimental approach is to

utilize, instead of avoiding, the nature that a diamond anvil cell generates nonhydrostatic stress to study the metallization of MoSe₂. Our geometry of the sample chamber and the nature of uniaxial stress can make the sample's region reach a quasi-homogeneous pressure distribution for performing reliable X-ray diffraction and Hall effect measurements.

3. RESULTS AND DISCUSSION

Figure 1 shows the isobaric temperature dependence of electrical resistivity in the temperature range of 80–290 K.

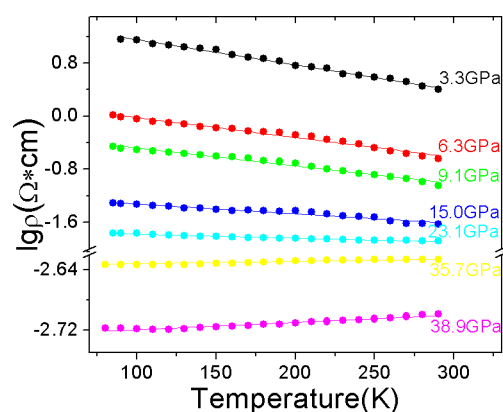


Figure 1. Temperature dependence of the resistivity of MoSe₂ at representative pressures.

The temperature (T)–resistivity (ρ) curves exhibit a linear relationship. At lower pressures (<35.7 GPa), the electrical resistivity of MoSe₂ demonstrates typical semiconductor characteristics, showing a constant decreasing trend with increasing temperature. The decreasing rate tends to be reduced, even approaching zero at around 35.7 GPa. At pressures above 35.7 GPa, a positive temperature dependence is observed, indicating the initiation of metallization of MoSe₂. Compared with the metallization of a single-crystal MoSe₂ reported above 40 GPa under hydrostatic compression using cubic BN as a pressure-transmitting medium,¹⁶ such result shows that the initiation pressure of metallization under nonhydrostatic conditions is lower than that under hydrostatic conditions.

To gain deeper insight into the anisotropic-stress-induced metallization and the carrier transportation for MoSe₂, nonhydrostatic compression Hall effect measurements were also conducted. As shown in Figure 2, at ambient conditions, the electrical resistivity, carrier concentration, and mobility are 30.1 $\Omega\text{-cm}$, $6.57 \times 10^{15} \text{ cm}^{-3}$, and $31.57 \text{ cm}^2 \text{ V}^{-1} \text{ s}^{-1}$, respectively. The magnitude of ρ and n in our experiments is comparable with previous results.¹⁴ As shown in Figure 2a, the resistivity of MoSe₂ decreases considerably by more than 4 orders of magnitude when the pressure was increased from ambient to 34.2 GPa. The resistivity of MoSe₂ then changes its pressure dependence at ~ 35.7 GPa and decreases gradually to 38.8 GPa. During decompression, following a hysteresis cycle, the abnormal change reemerges at 26.5 GPa, and resistivity does not get restored to its original magnitude at ambient conditions.

As shown in Figure 2b,c, from an ambient condition to 34.2 GPa, the carrier concentration increases by more than 5 orders of magnitude, while carrier mobility decreases smoothly. The increased carrier concentration can only be partly compensated

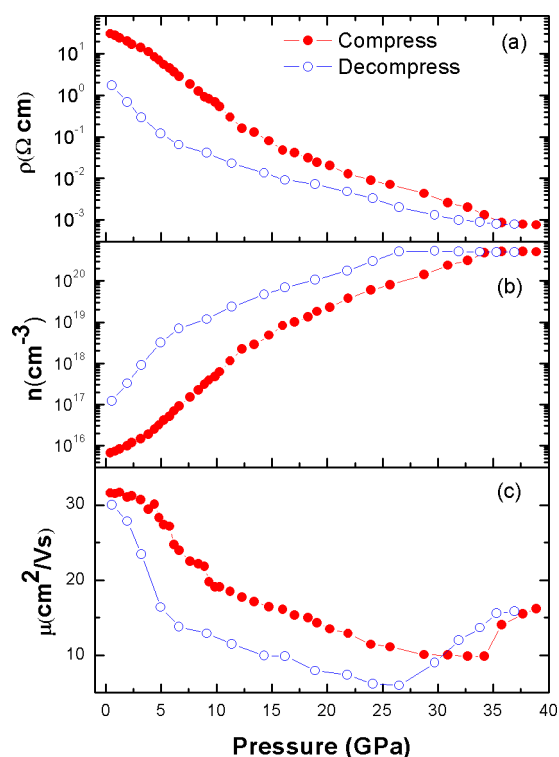


Figure 2. Electrical resistivity (a), carrier concentration (b), and mobility (c) of MoSe₂ as a function of pressure at room temperature.

by the decreased carrier mobility, which is the primary cause of dramatic reduction of electrical resistivity below 34.2 GPa. Upon further compression, both carrier concentration and mobility show abnormal changes at ~ 35.7 GPa. Carrier mobility inverts to positive pressure dependence while the carrier concentration seems to reach saturation. Consequently, the electrical resistivity of MoSe₂ decreases smoothly above 35.7 GPa. During decompression, both carrier concentration and mobility of MoSe₂ change abnormally at 26.5 GPa and do not get restored to their initial values when quenched to ambient conditions due to the hysteresis effect.

In order to understand the structural change in non-hydrostatic conditions, XRD measurements were carried out to monitor the structural variation of MoSe₂. Figure 3a shows the selected XRD patterns of MoSe₂ with no pressure-transmitting medium. At initial pressure of 1.4 GPa, the pattern of MoSe₂ can be well indexed into the 2H hexagonal layered crystal structure (*P*6₃/*mmc*), as seen in the previously reported result under hydrostatic pressure.¹³ It is discovered that, with increasing pressure, the diffraction lines continuously shift to larger 2θ values due to contraction of the lattice. No new peak is observed in the pressure range of the experiment. The pressure dependence of the lattice parameters is presented in Figure 3b. The cell parameters show a smooth continuous decrease with increasing pressure and also show no evidence for a phase transition under nonhydrostatic compression. The *a*-axis decreased by 6.9% and the *c*-axis decreased by 11.1% at 36.4 GPa, which indicates more typically anisotropic compression behavior under nonhydrostatic conditions. The cell parameters are in agreement with those of ref 13. Note that for MoSe₂ under hydrostatic and nonhydrostatic compression, the *c*-axis is much more compressible than the *a*-axis. The width of diffraction lines at nonhydrostatic compression is larger than that obtained at hydrostatic compression. More

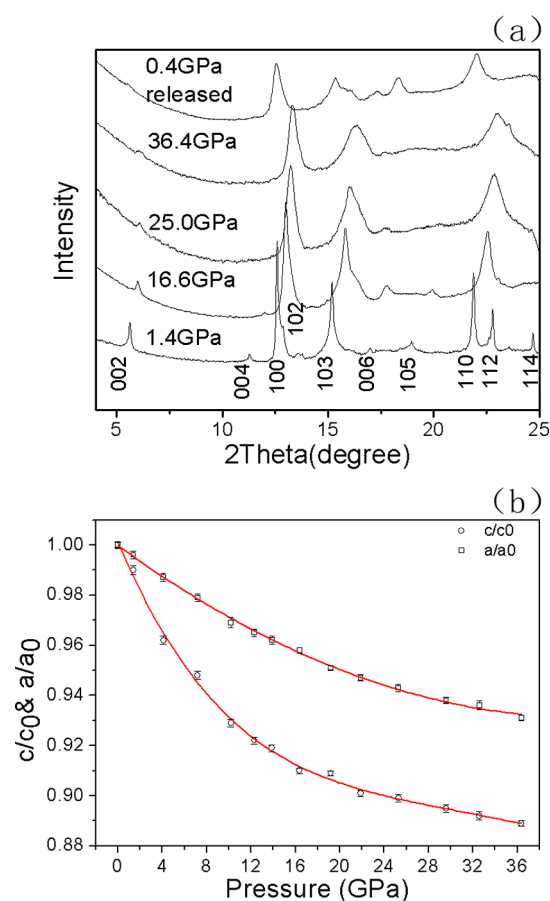


Figure 3. (a) Representative XRD patterns at various pressures with no pressure medium and (b) pressure dependence of the unit cell parameter. The errors within the symbols were received from the refinement of cell parameters.

severe pressure-induced line broadening is observed with anisotropic-stress elevation. Such behavior is ascribed to two sources, anisotropic-stress-induced comminution and micro-strain of sample crystallites. Since the introduction of anisotropic stress usually results in the comminution of the crystallites, such phenomenon effectively reduces the coherent scattering domain size of the sample and contributes to line broadening. Furthermore, the line broadening is also enhanced by the appearance of the microstrains in the crystallites under nonhydrostatic compression.²⁶ During decompression, diffraction peaks are gradually restored to their original position, while the broadened peak width is maintained, indicating that the comminution of the MoSe₂ crystallites after anisotropic-stress treatments is not recovered. The XRD results with no pressure medium show that no structural transformation had occurred in this pressure range, which also corresponds to similar observations with a neon pressure medium.¹⁶ Therefore, it is clear that an isostructural metallization process in powder MoSe₂ occurred under nonhydrostatic pressure.

The metallization caused by isotropic stress was first discovered by Mott²⁷ and has been known as the Mott transition. In Mott transition, pressure triggers the wave functions of the valence electrons to overlap, which results in the closing of the valence-conduction band gap and thus metallization. In general, for the semiconductor, the increase in pressure leads to a phenomenon named stress-induced impurity levels, in which atoms deviate from their equilibrium

positions and bring about additional energy levels in band gaps. At high pressure, the electric conduction is dominated by carriers from both over the full band gaps and the stress-induced impurity levels in the band gaps.²⁸ Such model of stress-induced ionization of impurity levels is usually utilized to understand the effect of hydrostatic pressure on the electrical properties of a semiconductor.²⁹ On the other hand, high pressure also makes conduction and the valence bands to broaden and the band gap to become narrow (as indicated by E_g' shown in Figure 4). Thus, more carriers can be activated

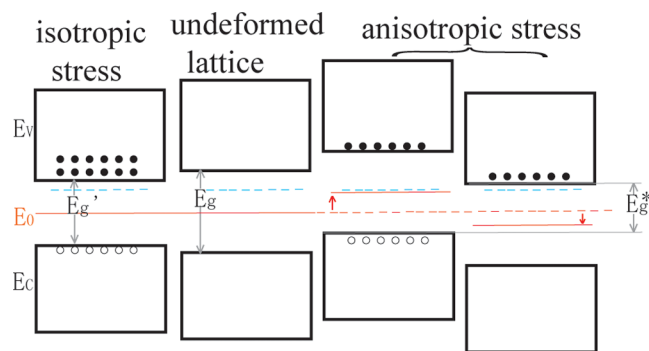


Figure 4. Sketch for the shift of the energy level under various kinds of stresses.

from a valence band to a conduction band. Therefore, the increase of the carrier concentration of MoSe_2 with increasing pressure up to 35.7 GPa is caused by both band gap narrowing and stress-induced impurity levels in band gaps. Above 35.7 GPa, the saturated carrier concentration suggests that the impurity levels are wholly ionized and bands completely overlap at higher pressure.

Unlike hydrostatic compression that compresses all three principal axes of a crystal lattice, nonhydrostatic compression tends to compress fewer lattice axes. Therefore, nonhydrostatic compression results in the deformation of Brillouin zone boundaries and shift of band gap mid-point E_0 . As a result, the indirect band gap shrinks to E_g^* ($E_g^* < E_g'$), as shown in the right part of Figure 4. Thus, nonhydrostatic compression can also close the band gap indirectly, even with smaller magnitude of stress. When the strain becomes large enough to close the gap, the bonding electrons delocalize and transform into the antibonding states. That is to say, the activation energy for transformation becomes zero. Therefore, under nonhydrostatic conditions, metallization of MoSe_2 can be initiated at lower pressure of 35.7 GPa.

4. CONCLUSIONS

In summary, we have performed *in situ* temperature-dependent electrical resistivity measurements, Hall effect measurements, and X-ray diffraction measurements on MoSe_2 under nonhydrostatic compression. The results demonstrate that the metallization of MoSe_2 occurs at a reduced pressure of 35.7 GPa compared to that under hydrostatic compression. Such observation suggests that the pressure requirement of isostructural metallization under nonhydrostatic conditions is lower than that under hydrostatic conditions (>40 GPa). Hall effect measurements showed that the dramatic reduction of electrical resistivity below 34.2 GPa is caused by an increased carrier concentration and gradual descent of electrical resistivity of the metallic phase of MoSe_2 due to the saturation

of stress-induced ionization. Under nonhydrostatic conditions, anisotropic stress can close the band gap more efficiently than that under hydrostatic compression because of the anisotropic-stress-driven deformations of Brillouin zone boundaries.

AUTHOR INFORMATION

Corresponding Authors

Bao Liu – College of Science, Northeast Electric Power University, Jilin 132012, China; orcid.org/0000-0001-8203-7955; Phone: +86-(0)432-6480-6621; Email: liubao@neepu.edu.cn

Chunxiao Gao – State Key Laboratory of Super Hard Materials, Jilin University, Changchun 130012, China; orcid.org/0000-0001-5329-2623; Phone: +86-(0)431-8516-8878-601; Email: cc060109@qq.com

Authors

Lin Lin – Department of Mechanical Engineering, Texas Tech University, Lubbock, Texas 79409, United States

Yang Gao – Department of Mechanical Engineering, Texas Tech University, Lubbock, Texas 79409, United States; Center for High Pressure Science and Technology Advanced Research, Shanghai 201203, China; orcid.org/0000-0003-4530-8570

Yanzhang Ma – Department of Mechanical Engineering, Texas Tech University, Lubbock, Texas 79409, United States

Pengyu Zhou – College of Science, Northeast Electric Power University, Jilin 132012, China

Dandan Han – College of Science, Northeast Electric Power University, Jilin 132012, China

Complete contact information is available at:

<https://pubs.acs.org/10.1021/acs.jpcc.1c00279>

Notes

The authors declare no competing financial interest.

ACKNOWLEDGMENTS

The authors thank scientists at Beamline 4W2 of BSRF for their technical help. This work was supported by the National Natural Science Foundation of China (Grant Nos. 11304034 and 11804047), the Science and Technology Development Program of Jilin City (Grant No. 201831733), and the Development Program of Education Department of Jilin Province (Grant No. JJKH20180425KJ).

REFERENCES

- (1) Kertesz, M.; Hoffmann, R. Octahedral vs. trigonal-prismatic coordination and clustering in transition-metal dichalcogenides. *J. Am. Chem. Soc.* **1984**, *106*, 3453–3460.
- (2) Jamison, W. E.; Cosgrove, S. L. Friction Characteristics of Transition-Metal Disulfides and Diselenides. *ASLE Trans.* **1971**, *14*, 62–72.
- (3) Voiry, D.; Yamaguchi, H.; Li, J.; Silva, R.; Alves, D. C. B.; Fujita, T.; Chen, M.; Asefa, T.; Shenoy, V. B.; Eda, G.; Chhowalla, M. Enhanced catalytic activity in strained chemically exfoliated WS₂ nanosheets for hydrogen evolution. *Nat. Mater.* **2013**, *12*, 850–855.
- (4) Cheng, L.; Huang, W.; Gong, Q.; Liu, C.; Liu, Z.; Li, Y.; Dai, H. Ultrathin WS₂ nanoflakes as a high-performance electrocatalyst for the hydrogen evolution reaction. *Angew. Chem., Int. Ed.* **2014**, *53*, 7860–7863.
- (5) Tsai, M.; Su, S.; Chang, J.; Tsai, D.; Chen, C.; Wu, C.; Li, L.; Chen, L.; He, J. Monolayer MoS₂ heterojunction solar cells. *ACS Nano* **2014**, *8*, 8317–8322.

- (6) Liu, H.; Su, D.; Zhou, R.; Sun, B.; Wang, G.; Qiao, S. Z. Highly ordered mesoporous MoS₂ with expanded spacing of the (002) crystal plane for ultrafast lithium ion storage. *Adv. Energy Mater.* **2012**, *2*, 970–975.
- (7) Najmaei, S.; Liu, Z.; Zhou, W.; Zou, X.; Shi, G.; Lei, S.; Yakobson, B. I.; Idrobo, J.-C.; Ajayan, P. M.; Lou, J. Vapour phase growth and grain boundary structure of molybdenum disulphide atomic layers. *Nat. Mater.* **2013**, *12*, 754–759.
- (8) Aruchamy, A.; Agarwal, M. Materials Aspects of Layered Semiconductors for Interfacial Photoconversion Devices. In *Photoelectrochemistry and Photovoltaics of Layered Semiconductors*; Springer, 1992; pp 319–347.
- (9) Reshak, A. H.; Auluck, S. Band structure and optical response of 2H–MoX₂ compounds (X = S, Se, and Te). *Phys. Rev. B* **2005**, *71*, No. 155114.
- (10) Galvan, D. H. Electronic structure calculations for MoSe₂ using extended huckel tight-binding method. *Mod. Phys. Lett. B* **2004**, *18*, 35–44.
- (11) Coehoorn, R.; Haas, C.; De Groot, R. Electronic structure of MoSe₂, MoS₂, and WSe₂. II. The nature of the optical band gaps. *Phys. Rev. B* **1987**, *35*, 6203.
- (12) Sugai, S.; Ueda, T. High pressure Raman spectroscopy in the layered 2H–MoS₂, 2H–MoSe₂, 2H–MoTe₂. *Phys. Rev. B* **1982**, *26*, 6554–6558.
- (13) Aksoy, R.; Selvi, E.; Ma, Y. X-ray diffraction study of molybdenum diselenide to 35.9 GPa. *J. Phys. Chem. Solids* **2008**, *69*, 2138–2140.
- (14) Dave, M.; Vaidya, R.; Patel, S.; Jani, A. High pressure effect on MoS₂ and MoSe₂ single crystals grown by CVT method. *Bull. Mater. Sci.* **2004**, *27*, 213–216.
- (15) Rifliková, M.; Martoňák, R.; Tosatti, E. Pressure-induced gap closing and metallization of MoSe₂ and MoTe₂. *Phys. Rev. B* **2014**, *90*, No. 035108.
- (16) Zhao, Z.; Zhang, H.; Yuan, H.; Wang, S.; Lin, Y.; Zeng, Q.; Xu, G.; Liu, Z.; Solanki, G. K.; Patel, K. D.; et al. Pressure induced metallization with absence of structural transition in layered molybdenum diselenide. *Nat. Commun.* **2015**, *6*, No. 7312.
- (17) Bissett, M. A.; Tsuji, M.; Ago, H. Strain engineering the properties of graphene and other two-dimensional crystals. *Phys. Chem. Chem. Phys.* **2014**, *16*, 11124–11138.
- (18) Duwal, S.; Yoo, C.-S. Shear-induced isostructural phase transition and metallization of layered tungsten disulfide under nonhydrostatic compression. *J. Phys. Chem. C* **2016**, *120*, 5101–5107.
- (19) Nayak, A. P.; Pandey, T.; Voiry, D.; Liu, J.; Moran, S. T.; Sharma, A.; Tan, C.; Chen, C.-H.; Li, L.-J.; Chhowalla, M.; et al. Pressure-Dependent Optical and Vibrational Properties of Monolayer Molybdenum Disulfide. *Nano Lett.* **2015**, *15*, 346–353.
- (20) Nayak, A. P.; Bhattacharyya, S.; Zhu, J.; Liu, J.; Wu, X.; Pandey, T.; Jin, C.; Singh, A. K.; Akinwande, D.; Lin, J.-F. Pressure-induced semiconducting to metallic transition in multilayered molybdenum disulphide. *Nat. Commun.* **2014**, *5*, No. 3731.
- (21) Chi, Z.; Zhao, X.; Zhang, H.; Goncharov, A. F.; Lobanov, S. S.; Kagayama, T.; Sakata, M.; Chen, X. Pressure-induced metallization of molybdenum disulfide. *Phys. Rev. Lett.* **2014**, *113*, No. 036802.
- (22) Gao, C.; Han, Y.; Ma, Y.; White, A.; Liu, H.; Luo, J.; Li, M.; He, C.; Hao, A.; Huang, X.; et al. Accurate measurements of high pressure resistivity in a diamond anvil cell. *Rev. Sci. Instrum.* **2005**, *76*, No. 083912.
- (23) Li, M.; Gao, C.; Ma, Y.; Li, Y.; Li, X.; Li, H.; Liu, J.; Hao, A.; He, C.; Huang, X. New diamond anvil cell system for in situ resistance measurement under extreme conditions. *Rev. Sci. Instrum.* **2006**, *77*, No. 123902.
- (24) Hu, T.; Cui, X.; Gao, Y.; Han, Y.; Liu, C.; Liu, B.; Liu, H.; Ma, Y.; Gao, C. In situ Hall effect measurement on diamond anvil cell under high pressure. *Rev. Sci. Instrum.* **2010**, *81*, No. 115101.
- (25) Li, M.; Gao, C.; Ma, Y.; Wang, D.; Li, Y.; Liu, J. In situ electrical conductivity measurement of high-pressure molten (Mg 0.875, Fe 0.125) 2 Si O 4. *Appl. Phys. Lett.* **2007**, *90*, No. 113507.
- (26) Singh, A. K.; Andrault, D.; Bouvier, P. X-ray diffraction from stishovite under nonhydrostatic compression to 70 GPa: Strength and elasticity across the tetragonal→ orthorhombic transition. *Phys. Earth Planet. Inter.* **2012**, *208–209*, 1–10.
- (27) Mott, N. F. The basis of the electron theory of metals, with special reference to the transition metals. *Proc. Phys. Soc. A* **1949**, *62*, 416–422.
- (28) Yao, M.; Wågberg, T.; Sundqvist, B. Effect of high pressure on electrical transport in the Li 4 C 60 fulleride polymer from 100 to 400 K. *Phys. Rev. B* **2010**, *81*, No. 155441.
- (29) Grant, A.; Griffiths, T.; Pitt, G.; Yoffe, A. The electrical properties and the magnitude of the indirect gap in the semi-conducting transition metal dichalcogenide layer crystals. *J. Phys. C: Solid State Phys.* **1975**, *8*, No. L17.